Preliminary Design and CFD Analysis of a Fire Surveillance Unmanned Aerial Vehicle

Luis E. Casas[1], Jon M. Hall[1], Sean A. Montgomery[1], Hiren G. Patel[1], Sanjeev S. Samra[1], Joe Si Tou[1], Omar Quijano[2], Nikos J. Mourtos[3], Periklis P. Papadopoulos[3]

Aerospace Engineering
San Jose State University
One Washington Square
San Jose, CA, 95192-0087

The Spartan Phoenix is an Unmanned Aerial Vehicle (UAV) designed for fire surveillance. It was inspired by the summer 2007 wildfires in Greece and California that caused billions of dollars in damage and claimed hundreds of lives. The Spartan Phoenix will map the perimeter of wildfires and provide real time feedback as to fire location and growth pattern. This paper presents the preliminary design of the UAV along with a CFD study of the horizontal and vertical stabilizers of the aircraft. Both surfaces use a NACA 0012 airfoil. First, the flow field over the airfoil was constructed using a CFD-GEOM grid. Next the grid was imported into CFD-FASTRAN and CFD-ACE to simulate a subsonic flow through the grid. The simulation was run using the Spartan Phoenix freestream conditions of 45 m/s airspeed at 0^0 angle-of-attack, and 20 m/s airspeed at 8^0 angle-of-attack, with pressure and temperature at 1 atm and 300 K respectively. The generated CFD solutions compared favorably to published data, solutions generated by the Institute of Computational Fluid Dynamics (iCFD), as well as results obtained from airfoil analysis using Sub2D, a potential flow simulation software.

Nomenclature

AR	*= aspect ratio*
α	*= angle of attack*
C_L	*= lift coefficient*
$C_{L,min}$	*= lift coefficient for minimum drag*
C_D	*= drag coefficient*
C_{Di}	*= induced drag coefficient*
C_{D0}	*= zero lift drag coefficient*
CG	*= center of gravity*
c	*= chord length*
e	*= Oswald efficiency factor*
L/D	*= lift-to-drag ratio*
UAV	*= Unmanned Aerial Vehicle*

I. Introduction

Every year wildfires claim lives and cause costly property damage worldwide. Wildfires are dynamic and can change direction and speed suddenly as wind conditions change. In the chaos and smoke generated by a large fire, it is not always easy to know where exactly the fire front is and in which direction it is moving. Lack of accurate information in these situations can be deadly. For example, in the 2007 fires in Greece, some evacuees were accidently directed towards the fire instead of away from it resulting in the tragic death of several people. This accident inspired the design of the fire surveillance UAV presented in this paper.

[1] BSAE student
[2] MSAE student
[3] Professor

The purpose of this UAV is to autonomously map the border of a wildfire and transmit the information to a ground station in real time, so that firefighting and evacuation efforts can be effectively coordinated. In the phase I of the project, the conceptual / preliminary design of the aerial vehicle was completed and a prototype was built and test-flown. The sensors necessary to carry out the mission of the UAV and the integration of the ground station will be selected and integrated in phase II. The Advanced Aircraft Analysis (AAA) software[1] was used in the preliminary design. Upon completion of the preliminary design, a CFD study of the flow around the empennage was performed to confirm the aerodynamic characteristics of the two surfaces (horizontal and vertical).

II. Preliminary Design

A. Mission Specification

Ideally, a fire surveillance UAV should be able to stay in the air for several days at a time, scanning the landscape for new fires, so that they can be detected and put out before they have a chance to grow, while autonomously avoiding terrain and other aircraft. A more realistic goal was chosen for phase I of this project, namely to design a prototype that will proof-of-concept.

Several questions arise when considering the operation of the UAV over a fire. For example, to detect a fire quickly and accurately is it better to fly low and follow the terrain or to loiter at high altitude and map the fire by simply panning the sensors? What sensor resolution is required? Should the UAV be able to descend quickly to inspect areas of interest (homes, fire crews, etc.) and then climb rapidly to make way for air tankers dropping retardant on the fire? Should it be able to withstand moderate turbulence? How will smoke affect the flight path of the UAV?

The hope is that the prototype (Spartan Phoenix) will help answer all these questions, while at the same time demonstrate the ability to fly autonomously and detect a fire. In particular, the prototype will be able to carry a large payload for an extended period of time, takeoff and land from a relatively short field, and climb quickly. Hence, the Spartan Phoenix mission requirements are:

Payload	= 8 lb
Range	= 180 nm
Endurance	= 4+ hours
Takeoff length	= 150 ft
Landing length	= 200 ft
Rate-of-climb	= 1,000 ft/min
Max cruise speed	= 75 mph

The relatively high endurance and climb rate requirements rule out electric propulsion for the Spartan Phoenix.

B. Configuration Design

The configuration of the Spartan Phoenix is shown in Figure 1. A pusher configuration was originally considered to allow better forward visibility for the sensors. However, the weight and balance analysis showed that this configuration could not be made longitudinally inherently stable because the payload did not weigh nearly as much as the payload (sensors). Hence, a more conventional tractor configuration was selected. The front location of the engine should not present a problem because the sensors will be pointed down towards the ground. The tractor configuration will also improve propeller efficiency as it provides cleaner airflow into the propeller and propeller ground clearance as it keeps the propeller far from the ground during the takeoff rotation.

A high wing configuration was selected, primary so that the fuel can be stored safely in the fuselage, directly under the wing, and close to the center of gravity. If the fuel were stored in the wing, sloshing in the fuel tanks would create large rolling moments and upset the flight path. Storing the fuel in the fuselage places it in a more centralized location, which significantly reduces sloshing. It should be kept in mind that the risk of a crash for our prototype is fairly high and placing the fuel tank in the fuselage offers an additional advantage in case of a crash, in that the nose will absorb some of the impact and will prevent the fuel tank from rupturing. Attaching the wings above the fuselage also provides more wingtip clearance from the ground, which helps avoid damage to the wings when landing on soft fields. An additional reason for the chosen configuration is also to keep the wing out of the way of the sensors, which are located in the belly of the fuselage.

A conventional tricycle landing gear was selected for improved ground stability and control along with a conventional empennage design. The latter makes it easier to design the plane with inherent longitudinal and directional stability for all flight conditions and this in turn facilitates the work of the autopilot.

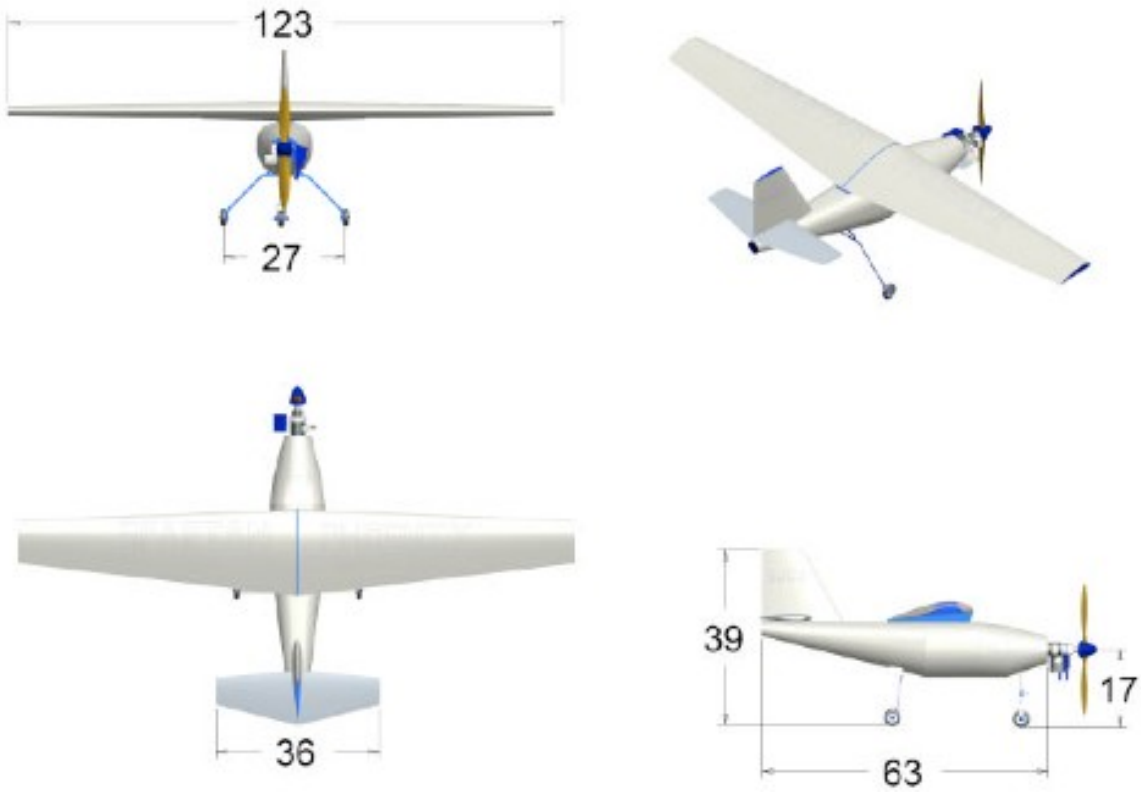

Figure 1 – A three-view drawing of the Spartan Phoenix showing the selected configuration (dimensions are in inches).

C. Weight Sizing

A database of UAVs with similar endurance and payload was compiled as a first step in preliminary weight sizing[2]. The takeoff weight was plotted against the empty weight and a line of best fit was constructed. This line gave us the lowest possible empty weight for a given takeoff weight based on current technologies. However, a takeoff weight of nearly 100 lbs was estimated from this method, which is not realistic for an aircraft the size of the Spartan Phoenix. This was due to the fact that most of the UAVs in our database were heavier aircraft carrying much more payload than the 8 lbs required for our mission.

The takeoff weight was estimated again using as a database remotely controlled (RC) airplanes from the SAE Aero Design Competition[3], as these airplanes are closer to the size of our UAV. The new database resulted in the more realistic estimate of 50 lbs for the takeoff weight. The amount of fuel required to fly for 4 hours was estimated from engine manufacturer fuel consumption data. A very conservative estimate of 12 lbs (approximately 2 gallons) was reached for the fuel weight. Allowing 8 lbs for payload and 12 lbs for fuel, the empty weight was estimated at 30 lbs. However, experienced remote control airplane builders suggested an empty weight of 24 lbs. Rather than

reducing our initial estimate, we allowed the extra 6 lbs as a margin for error in our structural weight due to lack of building experience.

D. Performance Sizing

A performance sizing analysis[1,2] determined the wing loading and power loading of the aircraft. Figure 2 shows the matching graph for the Spartan Phoenix with the performance requirements listed in the mission specification of the airplane.

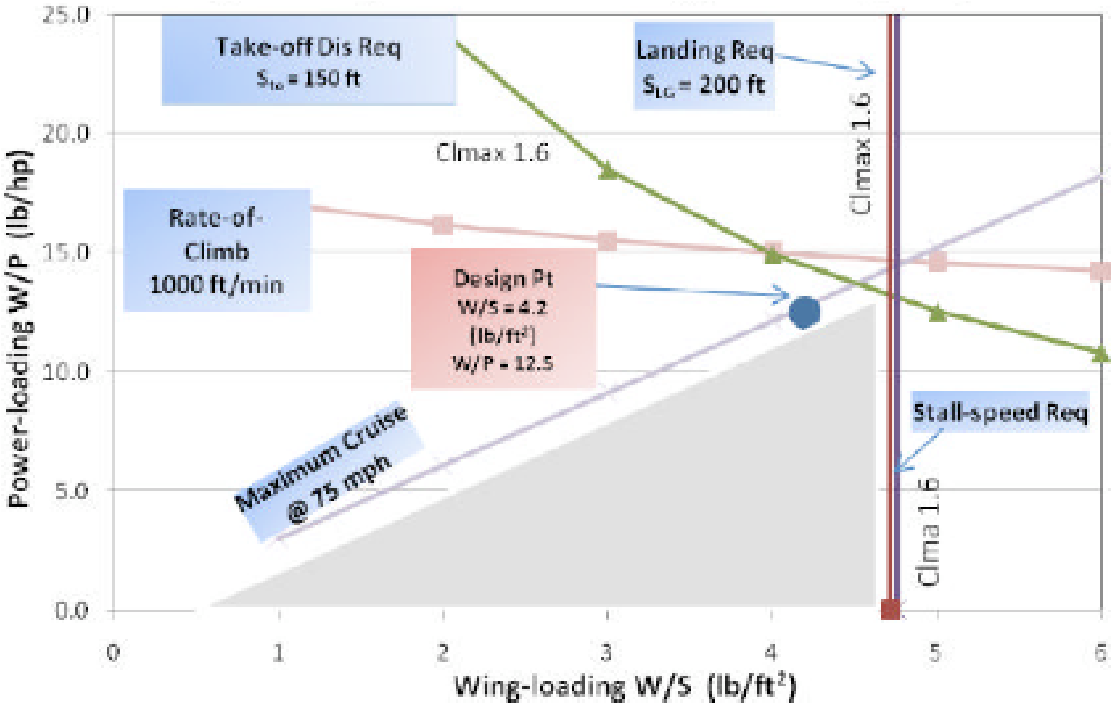

Figure 2 – Spartan Phoenix matching graph. The shaded area indicates all possible combinations of wing loading and power loading that meet all the performance requirements.

The highest possible wing loading and power loading that meet all the performance constraints were chosen, so that the plane is designed with the smallest wing and engine that will do the job. We assumed a maximum lift coefficient (C_{Lmax}) to be confirmed with a proper aerodynamic analysis of the wing. We selected this conservative value because the plane will not use any high-lift devices.

As can be seen in Figure 2, the highest wing loading that will meet all the performance requirements is 4.6 lb/ft^2 and the highest power loading is 14 lb/hp. Slightly more conservative values were chosen for the design point (4.2 lb/ft^2 wing loading and 12.5 lb/hp power loading). For our takeoff weight estimate of 50 lbs, this translates to a wing area of 12 ft^2 and a 4 hp engine.

Taking into consideration that small RC engine power ratings are typically inflated, the Zenoah G62, a 62 cm^3 displacement engine that runs on gasoline was selected. According to consumer reports this engine is highly reliable and has better cooling than other comparable engines, which is an important feature when flying in the hot air over a large fire. On the down side, the G62 weighs more than comparable engines.

E. Fuselage Design

The structural design of the fuselage is illustrated in Figure 3. A rib and spar structure was selected for the fuselage for its strength, rigidity, and the capacity to separate the fuselage into sections. The skin of the aircraft is composed of various fiberglass layers. Fiberglass is a lightweight composition material, which will add strength and protect the sensitive electronic equipment from hazardous weather conditions. The separation of sections by ribs helps isolate the cylindrical gas tank from the electronic components. The gas tank is supported by two ribs, which will prevent a gas leak from spreading into electronic equipment inside the fuselage.

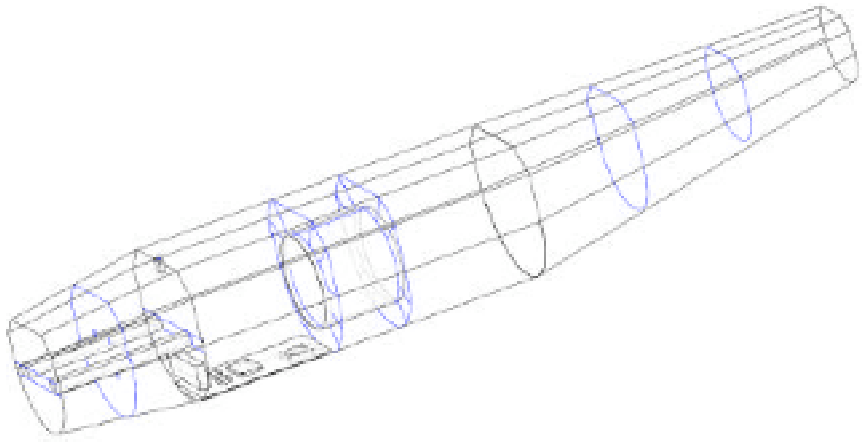

Figure 3 – Spartan Phoenix fuselage design, showing the structural layout, the payload, and the fuel tank.

The shape of the fuselage consists of a semicircle for the bottom surface, and a semi hexagon for the upper surface. A hexagon surface was chosen because it provides a flat surface to fasten the wing mounting structure to the fuselage. The fuselage is divided into three sections. The rear section attaches the empennage to the main structure of the aircraft. The main section houses the fuel tank and provides a rigid and flat structure for the wing. Finally, the front section holds the payload and the engine. A tapered cross-section from the main body of the fuselage to the rear and the front sections exists. The tapered cross-section from the main body to the nose is to accommodate the engine with a rigid and wrapped like structure, while the taper to the empennage yields sufficient ground clearance during take-off and landing. Finally, the tapered sections will keep the empty weight of the aircraft low.

F. Wing Design

A moderate wing aspect ratio of 8.33 was selected, as a compromise between low induced drag and vulnerability of the wings to damage. Hence, the wingspan is

$$b = \sqrt{AR \bullet S} = \sqrt{8.33(10)} = 10 \ ft \tag{1}$$

and the mean geometric chord is

$$\bar{c} = \frac{S}{b} = \frac{12}{10} = 1.2 \ ft \tag{2}$$

A taper ratio of 0.5 was chosen to improve the lift distribution and the maximum lift coefficient of the wing. The taper ratio also improves the aesthetic appearance of the airplane. The Advanced Aircraft Analysis (AAA) software[1] was used to calculate the maximum lift coefficient of the wing, which turned out to be 1.595 with an airfoil C_{lmax} of 1.7. The ailerons were sized based on relative aileron sizes of similar aircraft. The airfoil selected originally was the MomfoilC. This airfoil comes from a NASA mothership aircraft, which was used to lift a test vehicle up to altitude. The MomfoilC was chosen because of its good L/D ratio, high C_{lmax}, moderate pitching moment, and easy

to construct shape. The airfoil is thick which makes it easier to build with a strong and lightweight wing structure. Another feature of the MomfoilC is its flow separation on the lower surface at low lift coefficients, designed to create more drag for a faster descent. This will help the Spartan Phoenix descend in rapidly rising hot air over a fire. Flight tests will have to prove whether or not this is a useful feature for fire surveillance.

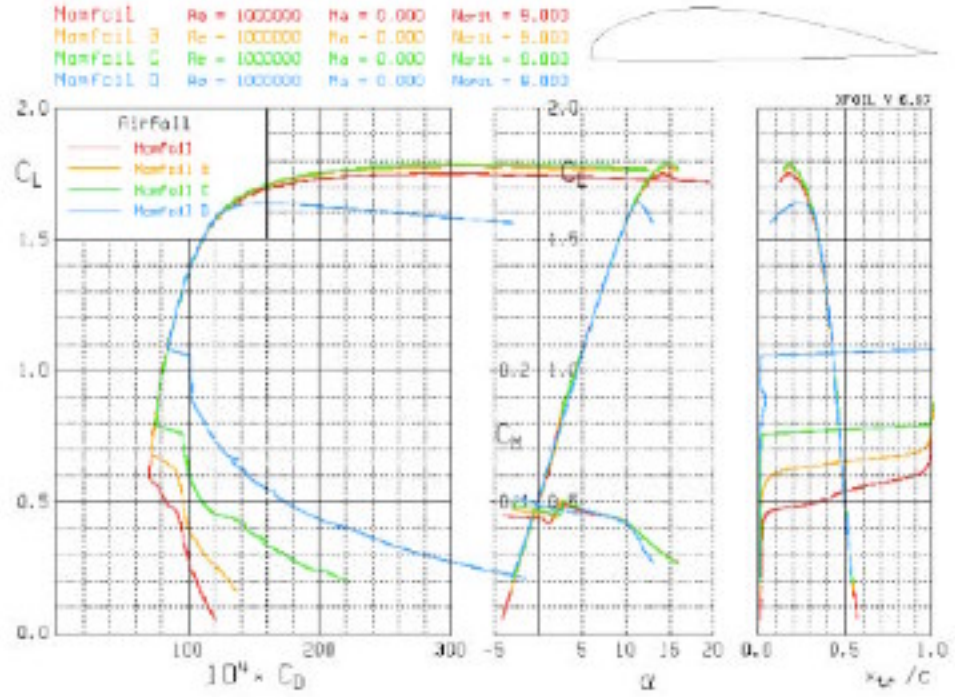

Figure 4 – Momfoil lift, drag, and pitching moment data generated with XFOIL software[4].

G. Empennage Design

The tail volume coefficient method[5] was used for the preliminary sizing of the empennage surfaces. Referencing our database of UAV data, a horizontal stabilizer volume coefficient of 0.46 and a vertical stabilizer volume coefficient of 0.03 were selected. The length of the aircraft is limited to 6 ft for easy transportation. This constraint determined the allowable moment arm of the empennage from the wing. The required surface area of the empennage was calculated at 2.5 ft^2 for the horizontal stabilizer and 1.5 ft^2 for the vertical stabilizer. The geometry of the empennage was chosen to match aircraft with similar configurations. The elevator was designed approximately one third of the horizontal stabilizer area to allow adequate control authority and the rudder approximately a quarter of the vertical stabilizer area. The complete empennage geometry is shown in Figure 5. The NACA 0012 airfoil was selected for both surfaces of the empennage.

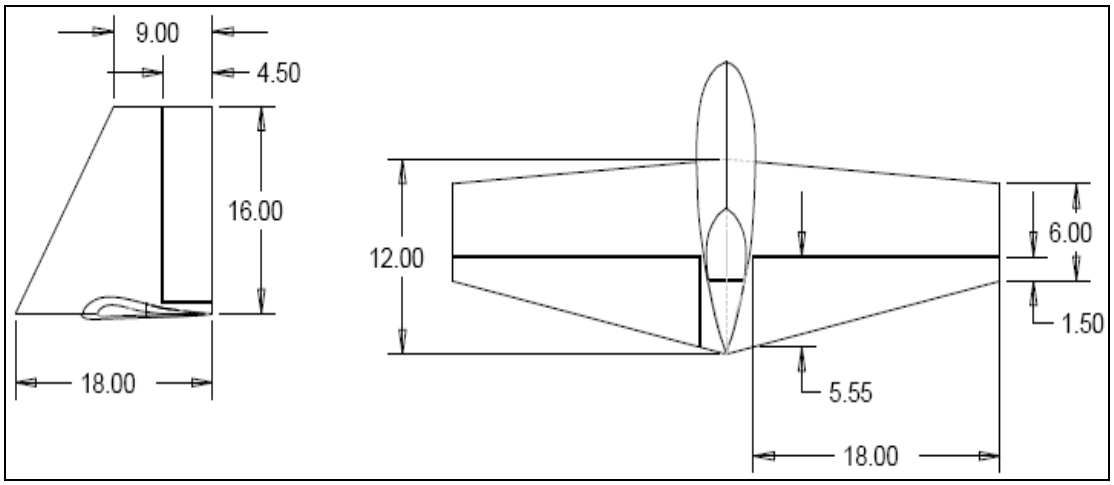

Figure 5 – Spartan Phoenix horizontal and vertical stabilizer geometry (dimensions shown in inches).

H. Landing Gear Design

A tricycle landing gear was selected for good ground stability and control. Considering the low cruise speed of the Spartan Phoenix a fixed landing gear was appropriate. The main gear is made of carbon fiber for strength and light weight. The nose gear is made of aluminum with a spring for shock absorption. The landing gear is designed to hold the fuselage 9 inches off the ground to provide adequate ground clearance. The prop has 6 inches of clearance from the ground. Because it is a tricycle gear, there are no prop clearance problems during rotation. The upsweep of the fuselage also provides adequate tail clearance. The main gear is significantly behind the aircraft CG to prevent tip over. The weight is approximately distributed evenly on each wheel.

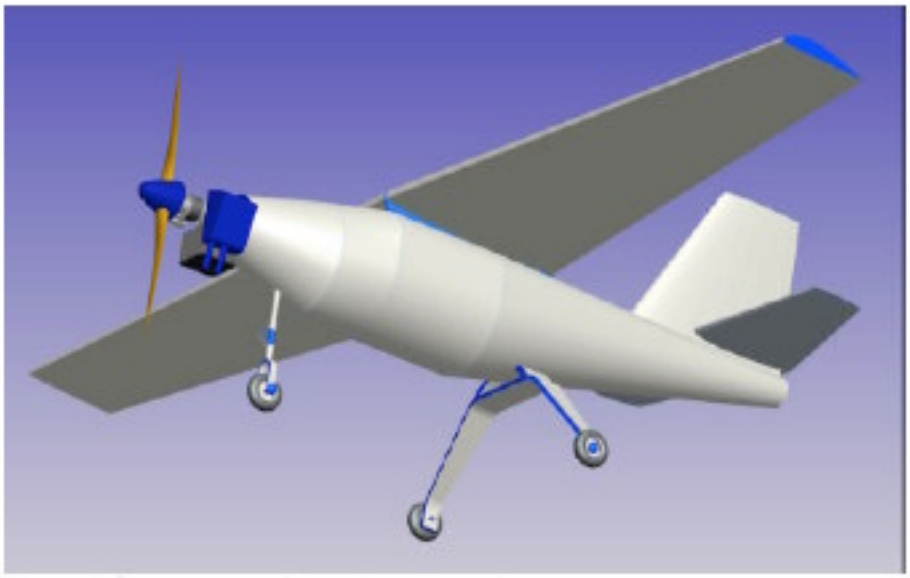

Figure 6 – Spartan Phoenix landing gear design.

I. Weight and Balance Analysis

The center of gravity (CG) location is critical for the stability and control of an aircraft. If the CG is too far aft, the aircraft will have low inherent stability and may even be inherently unstable. If the CG is too far forward, the aircraft will have high inherent stability, making control difficult. If the CG is off to one side or the other, a drag penalty is incurred to trim the resulting rolling moment. The height of the CG relative to the thrust line of the engine(s) affects the change in pitching moment due to power setting changes. All of these affects make it important to accurately determine the location of the CG. The center of gravity location for the fuel is placed close to the aircraft CG, so fuel burn does not cause significant CG travel. Table 1 lists the component weight brekdown and the estimation of the CG location for the UAV.

Table 1 – Spartan Phoenix component weight breakdown and CG estimation.

Component	Weight (lb)	CG X (ft)	CG Z (ft)
Datum		-2.0 (from nose)	-1.0 (from bottom of wheels)
Engine (including prop)	6.45	2.42	2.36
Main Wing	8.78	4.93	3.26
Fuselage	9.69	5.07	2.62
Horizontal Stabilizer	1.93	7.37	3.41
Vertical Stabilizer	0.81	7.29	3.84
Electronics Payload	4.5	3.5	2.25
Fuel	12.36	4.4	2.5
Nose Landing Gear	2.22	1.88	1.32
Main Landing Gear	1.24	5.5	1.39
Total	**50.00**	**4.36**	**2.60**

J. Stability and Control Analysis

The tail volume coefficient method for sizing the empennage is quick but it does not ensure a stable plane. To check the longitudinal stability of the UAV, the location of the aerodynamic center for the complete aircraft must be plotted as a function of horizontal stabilizer area and compared against the variation of the center-of-gravity location. To check the directional stability, the yawing moment stability derivative is plotted against sideslip angle. To determine the complete stability of the aircraft, all the stability derivatives need to be calculated and the longitudinal and lateral transfer functions analyzed to make sure the aircraft is stable in every mode (phugoid, short period, dutch roll, spiral, roll). The stability analysis in this section includes only the longitudinal and the directional modes.

The longitudinal stability of an airplane is determined by the distance between the center-of-gravity and the aerodynamic center. This distance expressed as a fraction of the mean aerodynamic chord, is known as the static margin of the airplane. The center-of-gravity must be ahead of the aerodynamic center for a longitudinally stable airplane. As the static margin increases, the longitudinal stability is increased, but maneuverability is decreased. To maintain a balance between controllability and maneuverability, airplanes typically have a static margin of 10%.

The center-of-gravity location is already known from the weight and balance analysis. The aerodynamic center of the wing is located at the quarter chord point. The other components that affect the location of the aircraft aerodynamic center are the fuselage and the horizontal stabilizer. The affect of the fuselage is usually destabilizing. In other words, the fuselage tends to move the aerodynamic center forward, reducing the static margin.

The estimated contribution of the fuselage on the aerodynamic center was calculated by following Munk's method, a common calculation used for manned aircraft. It was found that the fuselage reduced the static margin by 7%. The contribution of the horizontal stabilizer depends on the local flow around the tail. This is primarily influenced by the downwash from the wing, reducing the angle of attack on the horizontal stabilizer. Another affect on the tail is the propeller slipstream, which increases the dynamic pressure at the tail, making it more effective.

Most of the horizontal stabilizer surface area is in the propeller slipstream, so power has a large effect on the tail. The power setting for cruise was used for the aerodynamic center calculations.

Once the fuselage and horizontal stabilizer contribution are known, the aerodynamic center of the aircraft may be Calculated and plotted as a function of the horizontal stabilizer area. The center-of-gravity position used is the aft most because this is the most critical (lowest static margin). The center-of-gravity also varies with stabilizer area and it is assumed that the weight of the stabilizer increases proportionally with its area, moving the center-of-gravity aft. It was found that the static margin of the Spartan Phoenix for the horizontal stabilizer size determined from the tail volume method is 18%. This value is acceptable for the UAV because it provides enhanced stability, which is very important for flight in turbulent air over a fire. The longitudinal stability x – plot is shown in Figure 7.

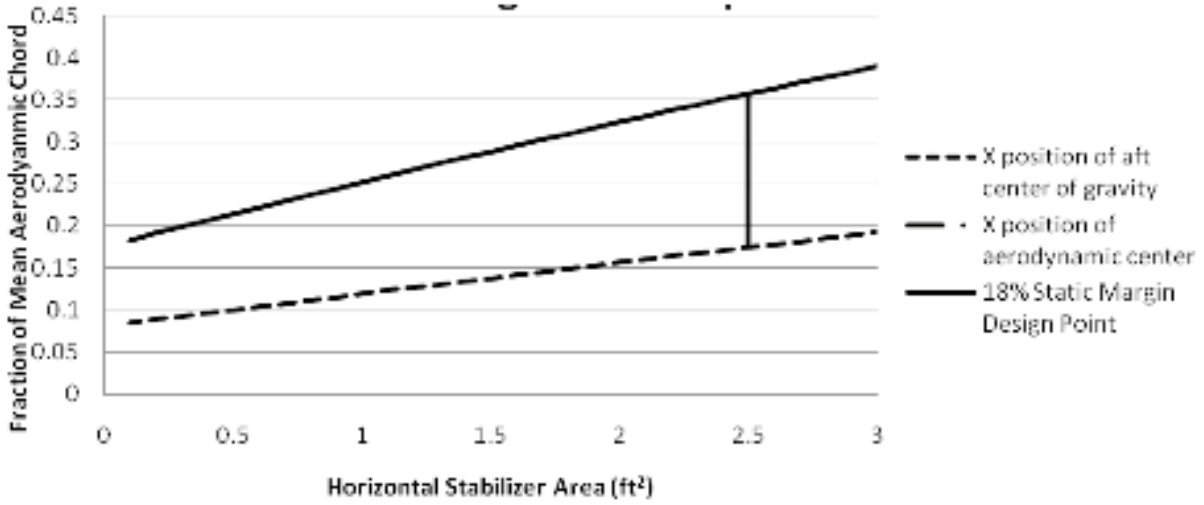

Figure 7 – Spartan Phoenix longitudinal stability x – plot.

The directional stability is determined by the yawing moment produced when the airplane sideslips. If this moment tends to decrease the sideslip angle, the airplane is directionally stable. The fuselage tends to destabilize the aircraft because it tends to diverge after a sideslip. The vertical stabilizer on the other hand, is the primary contributor to directional stability, hence the directional stability derivative is primarily a function of its size. The contributions of the fuselage and the vertical stabilizer were calculated and it was found that the directional stability was adequate (Figure 8).

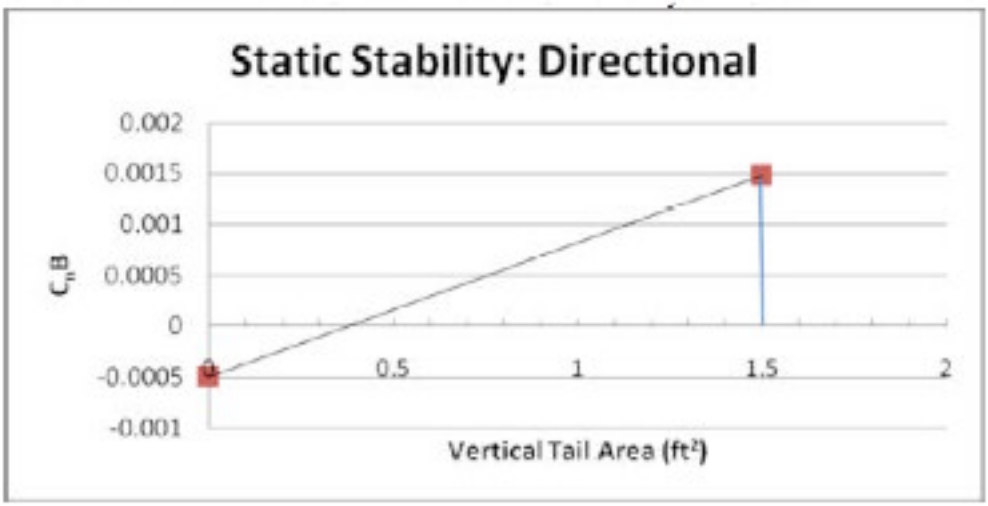

Figure 8 – Spartan Phoenix directional stability x – plot.

K. Drag Polar Estimation

It is important that the actual drag of the prototype closely matches the drag values assumed in the weight and performance sizing. The drag is broken down into two groups: zero-lift (profile) drag and drag due-to-lift (induced):

$$C_D = C_{D0} + C_{Di} = C_{D0} + K C_L^2 \tag{3}$$

The profile drag consists of skin friction drag and pressure drag. The coefficient of skin friction is determined from the Reynolds number. For the Spartan Phoenix, the boundary layer was assumed to be turbulent to account for the rough surfaces of the prototype. The landing gear drag was estimated from the range provided in reference [2], Table 3.6. An additional 0.025 miscellaneous drag was added to C_{Dmin} to account for other sources of zero-lift drag. This includes the radio antenna, the telemetry antenna, the video antenna, exposed servos and control fixtures, control surfaces gaps, interference drag, and separation drag. It is estimated that all of these sources combined contribute roughly as much drag as the landing gear. The Spartan Phoenix cruises at 45 mph, so compressibility drag is neglected. The resulting minimum drag coefficient is:

$$C_{D0} = 0.0853 \tag{4}$$

and the equivalent parasite area is:

$$f = 1.02\ ft^2 \tag{5}$$

Equation (5) indicates that the Spartan Phoenix has roughly as much profile drag as a one square foot plate placed perpendicular to the freestream. Considering that the maximum fuselage diameter is 1ft, the Spartan Phoenix is not very aerodynamic. However, the airplane will be flying at low speeds, hence the actual drag will be low.

The airplane drag polar is often written as:

$$C_D = \frac{\left(C_L - C_{L,\min}\right)^2}{\pi AR e} \tag{6}$$

where C_{Lmin} = 0.9, AR = 8.33, and e = 0.85 for the Spartan Phoenix. The drag polar is plotted in Figure 9. The curve appears to be relatively shallow because the aircraft drag is dominated by the profile drag. Most of the profile drag comes from the landing gear, engine, exposed antennas and exposed controls. Large drag improvements could be realized by fairing these areas. However, no fairings will be used in the prototype to simplify construction and improve accessibility.

The Spartan Phoenix is designed to cruise at C_L = 0.8 and this is close to the value for minimum drag. At this lift coefficient, C_D = 0.0858, and L/D = 9.3. A lift-to-drag ratio of 8.0 was assumed for the preliminary sizing. Hence there is a significant (14%) difference between assumed and calculated values of the lift-to-drag ratio. Normally, this requires a new design iteration, which will result in a lower airplane weight. However, no experimental data were available to validate our drag polar analysis and it is anticipated that the actual (flight) lift-to-drag ratio of the airplane will probably be somewhere between 9.3 and 8.0. The present analysis confirms that the Spartan Phoenix will be able to meet and more likely to exceed its mission requirements.

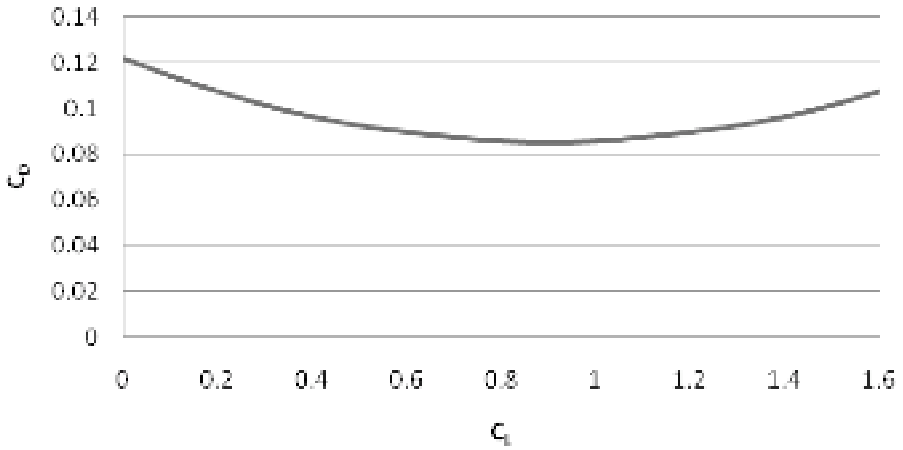

Figure 9 – Spartan Phoenix drag polar.

III. CFD Analysis of the Empennage

L. Computational Geometry and Grid Generation

Figure 5 shows the planform geometry for the horizontal and vertical stabilizer of the UAV. The airfoil length varies along the span of each surface due to sweep and taper. However, in our CFD analysis a constant length of one meter is assumed for both airfoils (horizontal and vertical). It follows that the maximum thickness of each airfoil is 12 cm.

The grid was generated using CFD-GEOM by importing the airfoil data from notepad. A tab file was created to import the data with 50 points along the shape of the airfoil and the points along the shape were connected using the spine tool to draw the airfoil on CFD-GEOM.

Figure 10 shows the overall view of the grid with data points and outer boundary designed to capture the flow characteristics. The leading edge region of the NACA 0012 is shown with grid spacing of 2×10^{-5} m and a stretching ratio of 1.5. The grid was generated with multiple variations of grid quality for trial and error cases to be run in ACE and/or FASTRAN. In order to capture the physics at the leading edge and along the contour of the airfoil grid, various sections were created with orthogonal grid spacing to capture the boundary layer near the wall. Figures 11 and 12 show the grid spacing and stretching ratio in the flow region near the leading edge.

However, the boundary layer was not captured very well because the number of iterations performed with FASTRAN and ACE was insufficient. It should be noted that our Reynolds number is very small compared to the Reynolds number in the published data used as benchmark. The initial grid was too coarse and had to be refined, so that all the flow characteristics were captured. At this point the simulation was run with 1,500 iterations and the solution started to converge. Once the number of iterations was increased, our results improved.

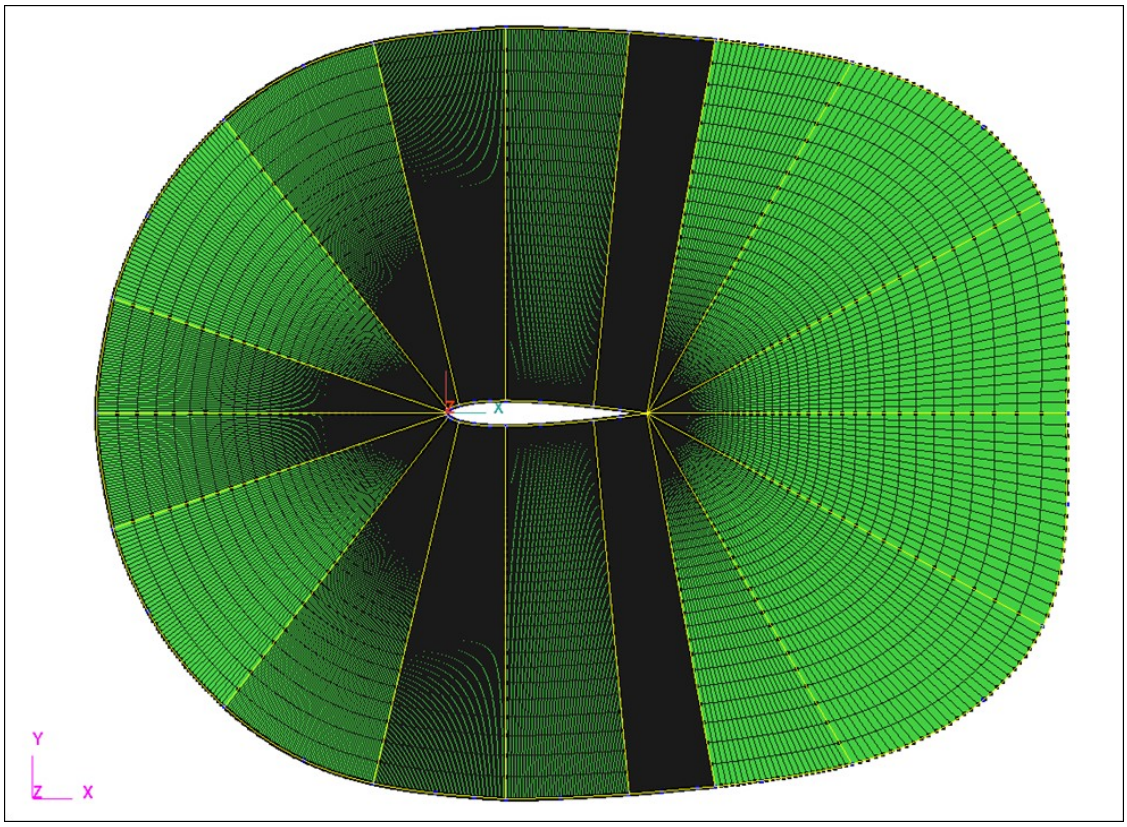

Figure 10 – NACA 0012 grid.

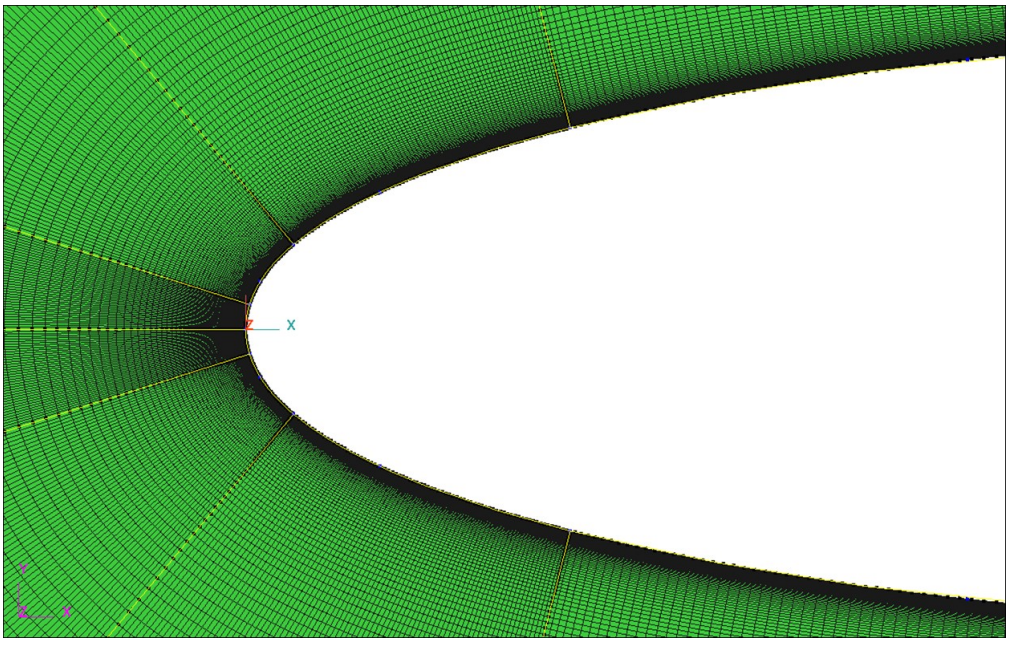

Figure 11 – NACA 0012 grid spacing for the leading edge region of the airfoil.

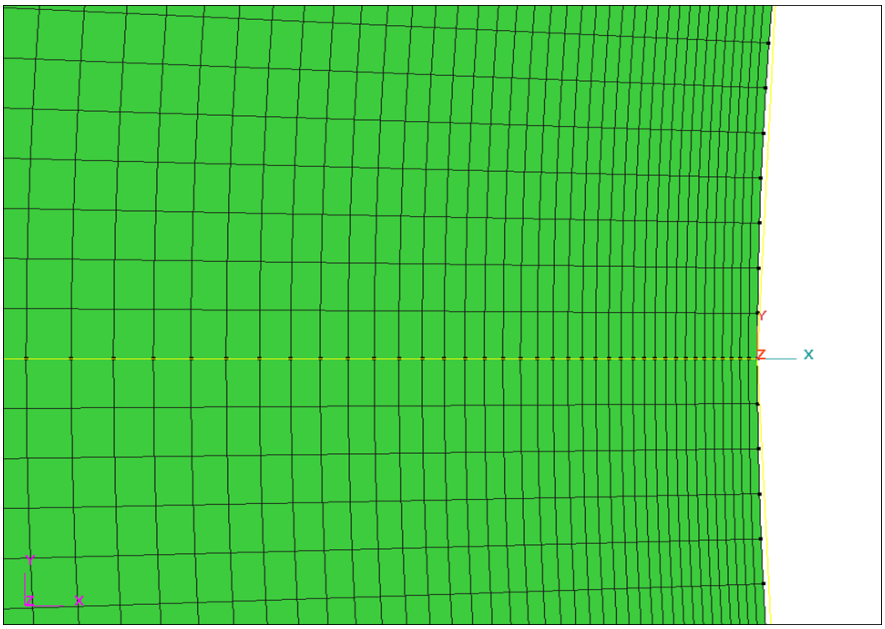

Figure 12 – NACA 0012 leading edge spacing and stretching ratio.

The trailing edge of the airfoil is another critical point and we had to provide additional grid points to capture the curvature of the flow, especially in the last 5% of the chord length. The trailing edge had hyperbolic grid spacing with a stretching ratio of 1.5 as shown in Figures 13 – 15. To provide good resolution it was divided into sections to ensure a smooth boundary.

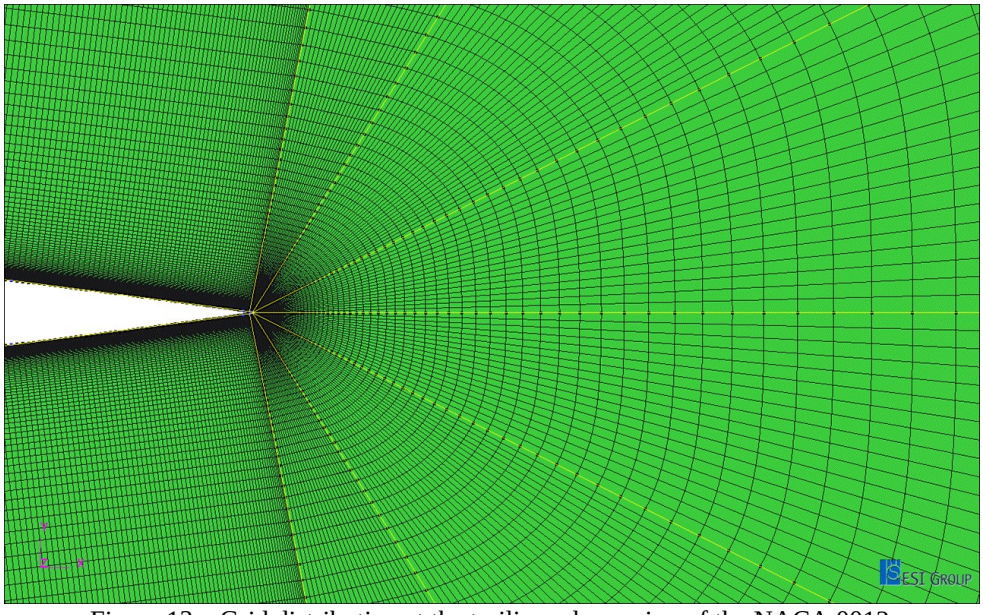

Figure 13 – Grid distribution at the trailing edge region of the NACA 0012.

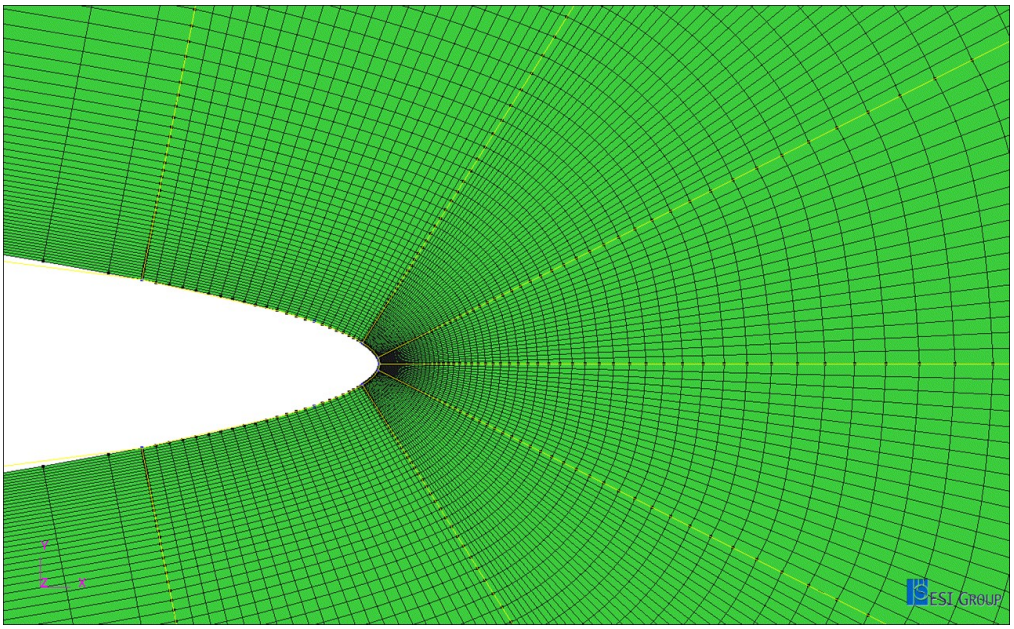

Figure 14 – Trailing edge geometry rounding to enable an O-Type grid.

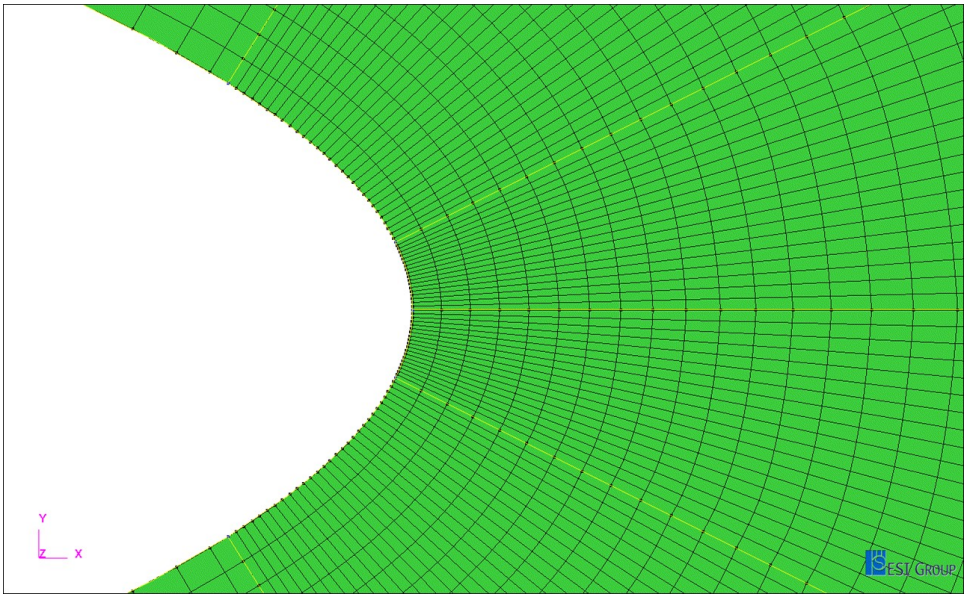

Figure 15 – Near wall grid spacing at the trailing edge of the airfoil.

M. CFD Results

On the first run FASTRAN and ACE were used with initial conditions 45 m/s and 20 m/s freestream velocity in the x-direction, a temperature of 300 K, and a pressure of 1 atm. Once satisfactory results for $\alpha = 0^0$ were obtained, the grid was refined in an effort to capture the physics of the flow around the airfoil more accurately. We ran three different angles-of-attack on ACE: 0 degrees, 8 degrees, and 12 degrees. However, ACE diverged for $\alpha = 12^0$ and a solution was not obtained. The ACE solution for $\alpha = 0^0$ was similar to the results obtained from Sub2D and the Institute of Computational Fluid Dynamics (iCFD). We benchmarked our results with respect to both programs.

Results for $\alpha = 0^0$

The velocity distribution from ACE for $\alpha = 0^0$ is shown in Figure 16. The pressure distribution for $\alpha = 0^0$ from ACE and Sub2D is shown in Figures 17 and 18 respectively. The iCFD solution is shown in Figure 19.

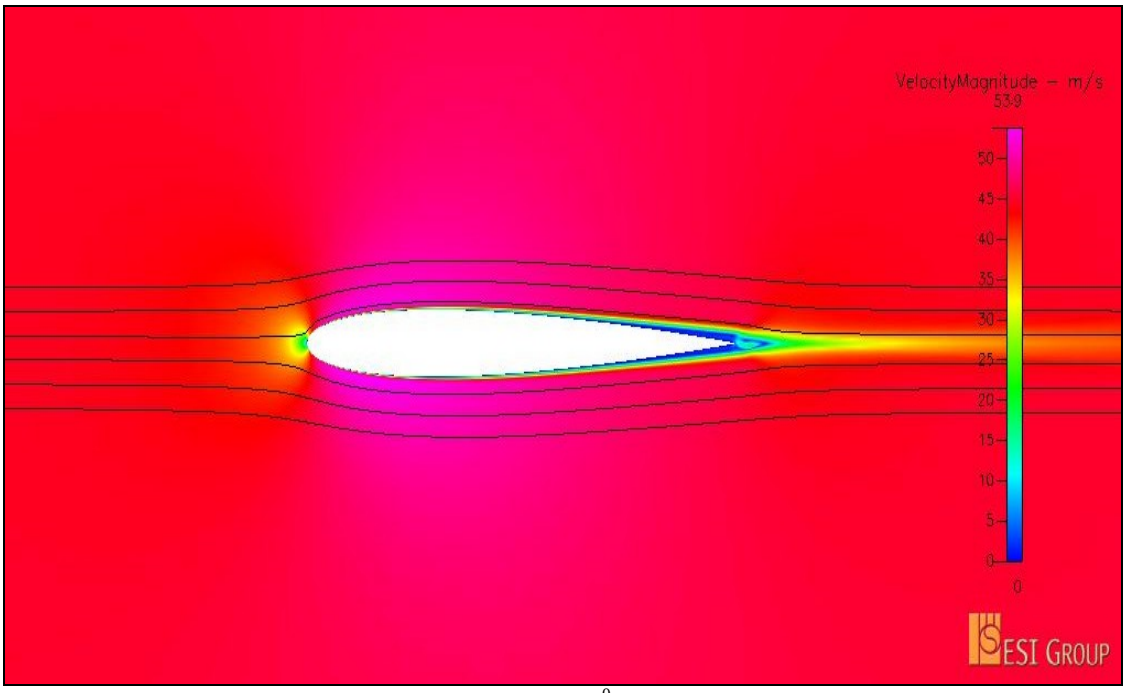

Figure 16 – Velocity distribution from ACE at $\alpha = 0^0$, with 1,500 iterations.

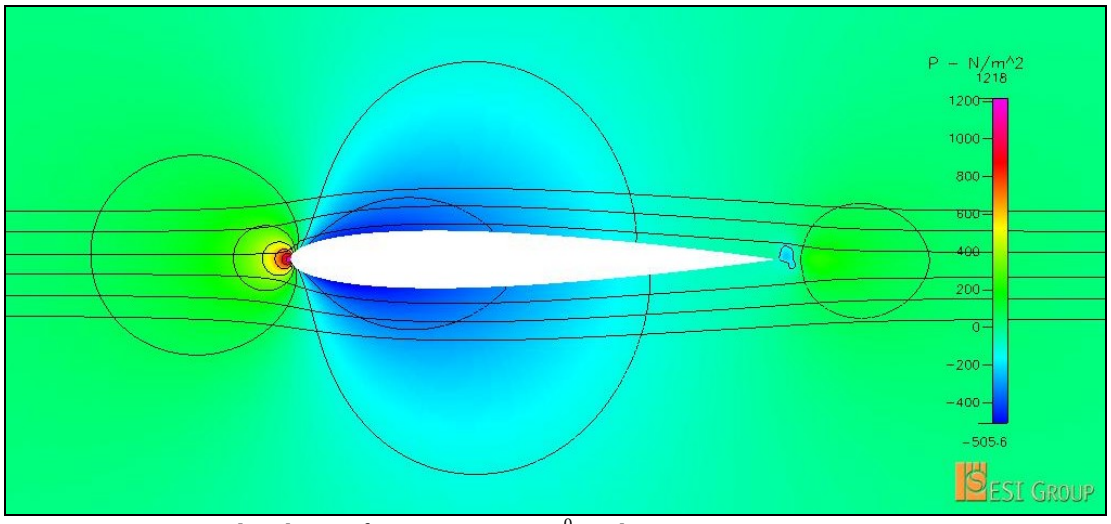

Figure 17 – Pressure distribution from ACE at $\alpha = 0^0$, with 1,500 iterations.

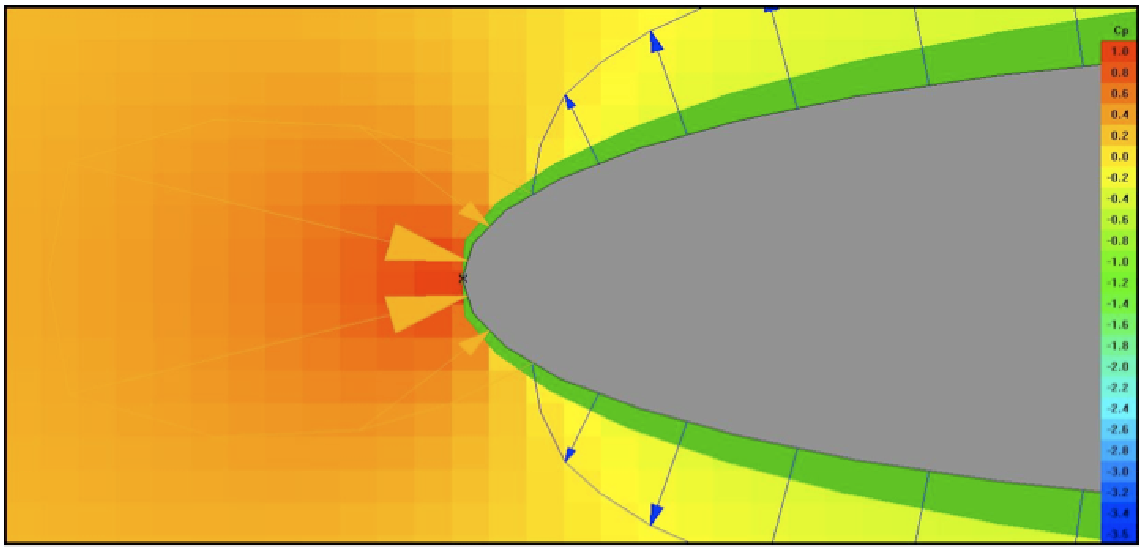

Figure 18 – Pressure distribution from Sub2D at $\alpha = 0^0$.

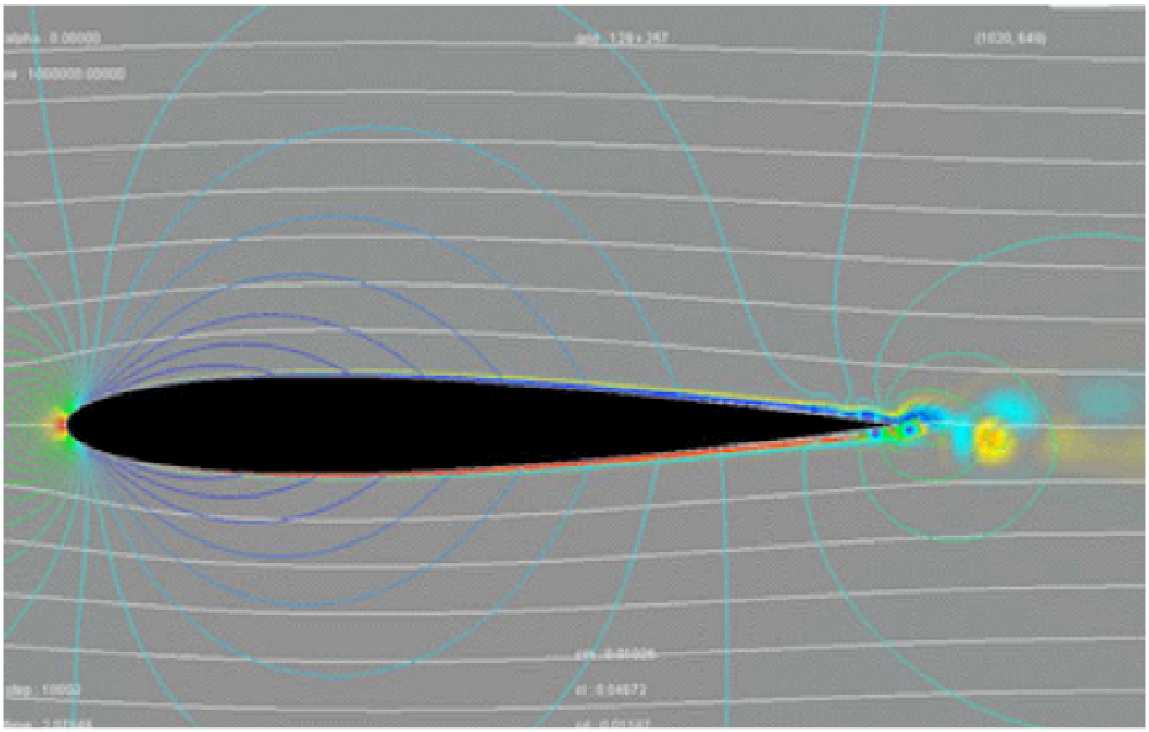

Figure 19 – Benchmark CFD simulation from iCFD at $\alpha = 0^0$.

Results for $\alpha = 8^0$

The velocity and pressure distributions from ACE for $\alpha = 8^0$ are shown in Figures 20 and 21 with 1,500 iterations and compare very well with Sub2D results shown in Figure 22.

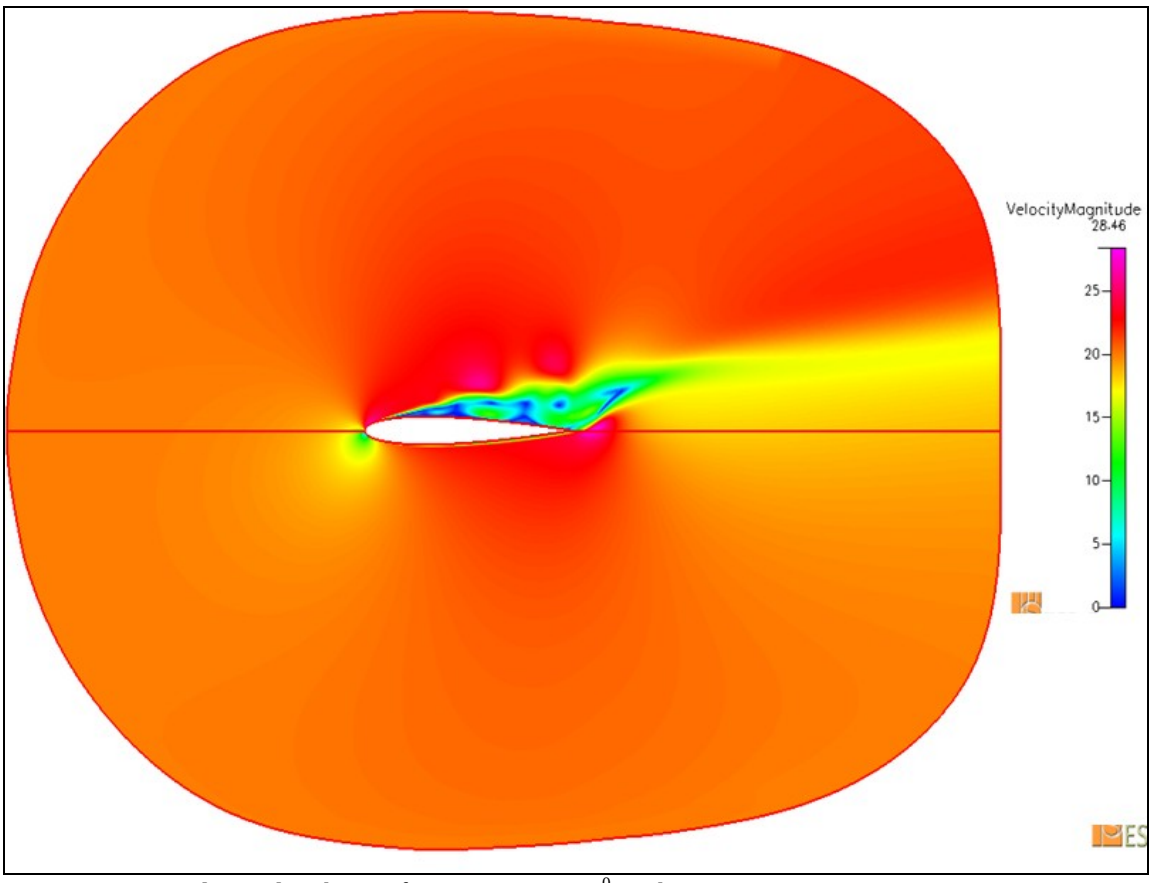

Figure 20 – Velocity distribution from ACE at $\alpha = 8^0$, with 1,500 iterations.

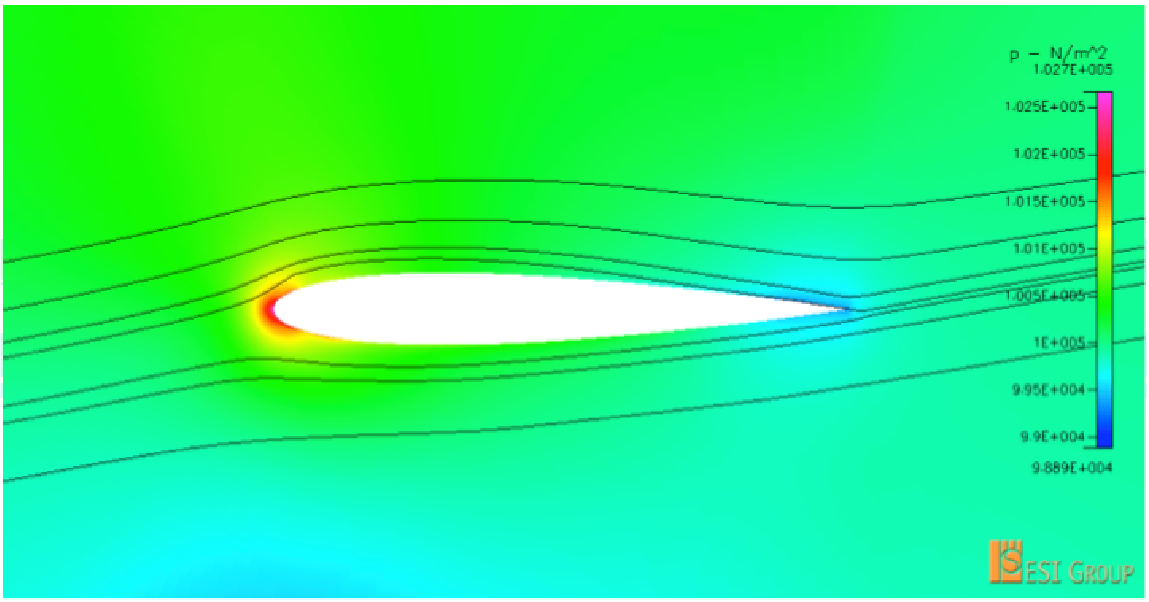

Figure 21 – Pressure distribution from ACE at $\alpha = 8^0$, with 1,500 iterations.

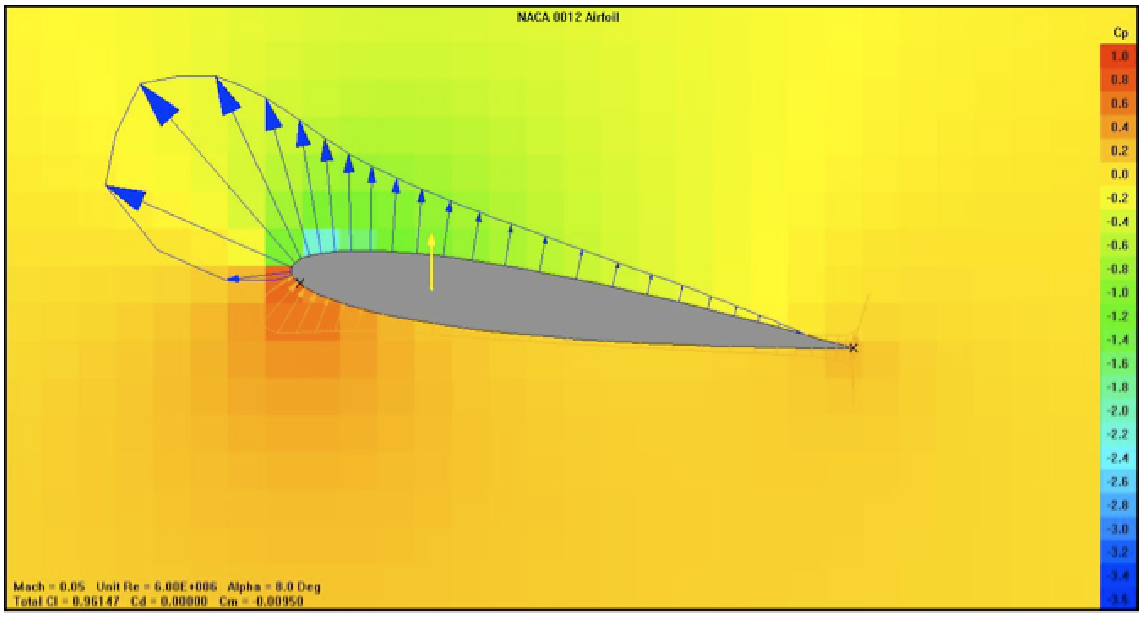

Figure 22 – Pressure distribution from Sub2D at $\alpha = 8^0$.

Sample calculations using Bernoulli's equation for $\alpha = 0^0$ and $\alpha = 8^0$ confirmed the stagnation pressures calculated in our CFD results.

IV. Conclusion

The purpose of this paper was to demonstrate the integration of modern computational tools in the preliminary design and analysis of a small UAV. In particular, the AAA program was used for a class I preliminary design[5]. One of the difficulties was that the databases in the AAA program do not include UAVs hence a new database had to be generated. However, most of the available UAVs are much larger in size than the one proposed in this paper and their data trends had to be interpreted with caution. Once the geometry of the UAV was determined with AAA, Sub2D and ACE were used for aerodynamic analysis of the empennage airfoils. The results were fairly good, however, more grid points were necessary to match with wind tunnel data and simulations performed in iCFD.

Acknowledgments

Special thanks to Steve Morris of the MLB Company for his generous donation of materials and to Dr. Periklis Papadopoulos for his guidance and support in the CFD analysis.

References

1. Advanced Aircraft Analysis software, DARcorporation, Lawrence, Kansas, URL: <http://www.darcorp.com/Software/AAA/>
2. Roskam, J., *Airplane Design pt. I: Preliminary Sizing of Airplanes*, DARcorporation, Lawrence, Kansas, 2005, URL: <http://www.darcorp.com/>
3. Society of Automotive Engineering Collegiate Design Series, URL: http://students.sae.org/competitions/aerodesign/
4. Drela, Marc, XFOIL Subsonic Airfoil Development System, URL: < http://web.mit.edu/drela/Public/web/xfoil/>
5. Roskam, J., *Airplane Design pt. II: Preliminary Configuration Design and Integration of the Propulsion System*, DARcorporation, Lawrence, Kansas, 2005, URL: <http://www.darcorp.com/>